J. Fluid Mech. (2002), *vol.* 470, *pp.* 359–382.
DOI: 10.1017/S0022112002002100 Printed in the United Kingdom

Experimental investigation on the secondary instability of liquid-fluidized beds and the formation of bubbles

By PAUL DURU AND ÉLISABETH GUAZZELLI
IUSTI, CNRS-UMR 6595, Technopôle Château-Gombert, 13453 Marseille cedex 13, France

(Received 3 December 2001 and in revised form 14 June 2002)

The objective of the present work is to investigate experimentally the secondary instability of the one-dimensional voidage waves occurring in two-dimensional liquid-fluidized beds and to examine the physical origin of bubbles, i.e. regions devoid of particles, which arise in fluidization. In the case of moderate-density glass particles, we observe the formation of transient buoyant blobs clearly resulting from the destabilization of the one-dimensional wavy structure. With metallic beads of the same size but larger density, the same destabilization occurs but it leads to the formation of real bubbles. Comparison with previous analytical and numerical studies is attempted. Whereas the linear and weakly nonlinear analytical models are not appropriate, the direct nonlinear simulations provide a qualitative agreement with the observed destabilization mechanism.

1. Introduction

The bubbling behaviour of gas-fluidized beds is one of the most intriguing phenomena occurring in fluidization. When a bed of solid particle is fluidized by a gas, regions almost completely devoid of particles, known as 'bubbles', appear near the bottom of the bed and rise, causing the bed to take on the appearance of a boiling liquid. Most of what has been learnt about such bubbles concerns the behaviour of single gas bubbles (see for instance the review of Davidson 1995). By contrast, liquid-fluidized beds are found to be less unstable and to develop much smoother structures, namely voidage waves, which have mostly been studied in narrow tubes (see Anderson & Jackson 1969; Ham *et al.* 1990; Nicolas *et al.* 1996; Duru *et al.* 2001). The question of the physical origin of the bubbles has only been addressed recently and, similarly, so has the search for a physical mechanism which would allow a clear distinction to be made between bubbling and non-bubbling fluidized beds and the difference between gas and liquid fluidization to be explained.

In a series of papers (Batchelor 1988, 1993; Batchelor & Nitsche 1991, 1993, 1994), Batchelor and Nitsche proposed a four-stage scenario to explain the formation of bubbles. First, a one-dimensional voidage wave evolves from the unstable uniform state and creates stratification of the suspension with alternating dilute and dense layers. Secondly, the one-dimensional wavetrain develops a two-dimensional structure because of a gravitational overturning instability, which tends to tilt 'heavy' layers of high particle concentration and 'light' layers of low particle concentration. Thirdly, this secondary instability ultimately creates regions of lower-than-average particle concentration where an internal fluid circulation develops. Particles are finally expelled by centrifugal forces from these buoyant blobs and this leads to bubbles of clear fluid rising up the bed.

There is now a general consensus on the two first stages proposed by Batchelor and Nitsche. Through a linear stability analysis of a two-phase model to describe the fluidized beds, Anderson & Jackson (1968) showed that fluidized beds are most unstable to one-dimensional vertically propagating disturbances. The resulting one-dimensional voidage wavetrain has been widely studied in experiments using narrow liquid-fluidized beds (see Anderson & Jackson 1969; Ham *et al.* 1990; Nicolas *et al.* 1996; Duru *et al.* 2001). This one-dimensional voidage wave has been shown to be unstable to two-dimensional perturbations of large wavelength. This unstable character has been established analytically by Göz (1995) and Göz & Sundaresan (1998) who studied the weakly nonlinear stability of small-amplitude one-dimensional waves to transverse two-dimensional perturbations.

Recent numerical studies, focusing on two-dimensional fully nonlinear simulations of the two-phase equations, have dealt with the situation obtained as a result of this two-dimensional destabilization. Anderson, Sundaresan & Jackson (1995) studied the evolution of two-dimensional disturbances applied to two different base states: the uniform bed and the fully saturated one-dimensional wavetrain. In both cases, they obtained bubble formation in their simulations of gas-fluidized beds, resulting either from the two-dimensional destabilization of the fully developed one-dimensional voidage wave or from the growth of a two-dimensional perturbation applied to the uniform bed.

When simulating a liquid-fluidized bed, Anderson *et al.* (1995) reported no bubble formation. The two different base states mentioned above in the case of gas-fluidized beds were examined as well. When a two-dimensional perturbation was allowed to develop, superimposed on a fully developed one-dimensional voidage wave, the evolution of the resulting two-dimensional structure created short-lived buoyant blobs which were rapidly destroyed because more particles entered them from their roof than were able to escape from their base. When a two-dimensional perturbation was imposed on the uniform bed, the destabilization of the plane wavetrain occurred as previously but earlier in the one-dimensional mode development so that the minimum particle concentration obtained in the buoyant blob was larger than previously. For this latter situation, Anderson *et al.* (1995) argued that the growth rates of the one-dimensional and two-dimensional instability were such that the one-dimensional instability failed to produce sufficient voidage gradients before the two-dimensional destabilization occurred, contrary to what is found for gas-fluidized beds.

Glasser, Kevredikis & Sundaresan (1996, 1997) have shown that bubble-like structures are two-dimensional stationary solutions of the two-phase equations, for all the cases studied, covering gas-fluidized beds as well as liquid-fluidized beds. Then, they checked whether these bubble-like structures could be reached by the destabilization either of the uniform bed or of the fully saturated one-dimensional wavetrain. Like Anderson *et al.* (1995), Glasser *et al.* (1996, 1997) obtained, through perturbation of both base states, bubble formation in their simulations of a gas-fluidized bed and a water-fluidized bed of dense lead shot beads. Their results obtained when simulating a liquid-fluidized bed of glass beads are less clear-cut. For high-amplitude two-dimensional solutions, their results are similar to those of Anderson *et al.* (1995) without bubble formation, but they note that low-amplitude two-dimensional stationary solutions can be reached by both mechanisms described above. Glasser *et al.* (1997) finally preferred to refer to a subtle difference in the solid flow pattern of the stationary two-dimensional structures to make a distinction between bubbling and non-bubbling beds.

The physical link with the scenario proposed by Batchelor and Nitsche is not

straightforward. Nonetheless, Anderson *et al.* (1995) and Glasser *et al.* (1996, 1997) have drawn attention to the similarity with the physical mechanism proposed by Batchelor & Nitsche (1991) for the initial buckling of the one-dimensional waves.

The two-dimensional destabilization of a plane wavetrain has been observed experimentally by El-Kaissy & Homsy (1976) with a two-dimensional liquid-fluidized bed of glass beads. The destabilization of the wavetrain resulted into the brief appearance of voidage pockets. These voidage pockets were short-lived and were far from being totally empty of particles. This is reminiscent of what was found by Anderson *et al.* (1995) and Glasser *et al.* (1997) and it is the only experimental observation supporting these simulation results. In a wider bed and larger range of fluidization, Didwania & Homsy (1981) identified four discrete regimes of fluidization including (in the order of increasing fluidization) wavy, transverse structure, turbulent, and bubbly states. There is also an older report of a three-dimensional bubbling liquid-fluidized bed of lead shot particles (Davidson & Harrison 1963) revealed by bubble eruption at the free surface, but nothing is said about the way these bubbles were formed. As far as we know, there is no quantitative experimental study of the destabilization of the one-dimensional wavetrain and of its possible link to bubble formation.

In this paper, we present results concerning the secondary instability of the one-dimensional voidage wavetrain occurring in two-dimensional liquid-fluidized beds. In the case of moderate-density glass beads, we describe the formation of transient buoyant blobs resulting clearly from the destabilization of the one-dimensional wavy structure, analogous to that qualitatively observed by El-Kaissy & Homsy (1976) and to that found in the numerical simulations. We also examine the mechanism of disappearance of these buoyant blobs. With metallic beads of the same size but larger density, we report, for the first time, on two-dimensional destabilization leading to the formation of real bubbles. We attempt to compare quantitatively these results to those of the recent numerical simulations.

In § 2 the experimental techniques are presented. The experimental results for the moderate-density particles are presented in § 3 and those for the high-density particles in § 4, including a detailed description of this new bubbling regime of liquid fluidization. The response of the bed to a single forced perturbation is briefly discussed in § 5. Comparisons with numerical and theoretical works are given in § 6. Conclusions are drawn in § 7.

2. Experimental techniques

2.1. *Experimental apparatus*

The fluidized bed apparatus was similar to that used by Duru *et al.* (2002). The one-dimensional bed was however replaced by a two-dimensional bed which consisted of a glass rectangular cell of 12×1.2 cm cross-section and 200 cm high, see figure 1. The suspension was held by a moving two-dimensional piston-injector based on that used in the one-dimensional experiments. However, because of strong friction, it was not possible to operate this piston to produce a local harmonic forcing of the particle concentration at the bottom of the bed, as done in one-dimensional experiments. This piston was thus used to study the response of the bed to a single forced perturbation, see § 5. A uniform distribution of the flow was produced by a bronze sintered plate located before the piston, which ensured a very large pressure drop across the distributor. The fluid was pure water. It was circulated through the bed by a piston metering pump (Fluid Metering Inc. model QD, 1425 r.p.m.), used to

Set	d_s (μm)	ρ_s (g cm^{-3})	W_b/d_s	D_b/d_s
A	1220 ± 60	4.08 ± 0.01	100	10
B	1200 ± 90	2.48 ± 0.01	100	10
C	1000 ± 40	7.96 ± 0.01	120	12
D	685 ± 40	2.55 ± 0.01	175	18

TABLE 1. Particle characteristics.

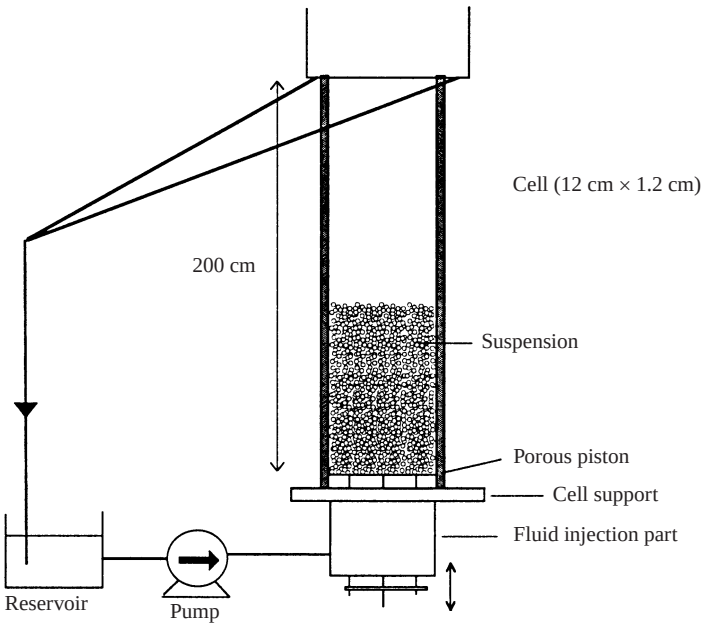

FIGURE 1. Experimental set-up. The cell support part is screwed on a fixed stand. The porous support of the beads can be moved.

produce flow rates up to 7 dm^3 min^{-1}. A soft tube was placed upstream of the bed in order to isolate the bed from pump vibrations. A soft tube also collected the overflow at the top of the bed and carried it back to a thermostated reservoir. The water temperature was maintained at $27 \pm 1\,^{\circ}$C and the viscosity and density of the fluid were $\eta_f = 0.90 \pm 0.02$ cP and $\rho_f = 0.997 \pm 0.002$ g cm^{-3}. The particles used were spherical glass beads or stainless steel beads, see table 1. Whereas the bead diameter was roughly the same for sets A, B and C, the densities varied from 2.48 g cm^{-3} to 7.96 g cm^{-3}, see table 1. The bed depth to particle diameter ratio D_b/d_s and the bed width to particle diameter ratio W_b/d_s are also given in table 1.

2.2. *Volume fraction measurements*

With glass beads, we were able to study the light transmitted through the bed by using a charged coupled device camera (768×512 pixels) and the public domain image processing NIH Image†. The fluidized bed was backlighted by using two neon

† Public domain NIH Image program, developed at the U.S. National Institute of Health and available from the Internet by anonymous ftp from zippy.nimh.nih.gov.

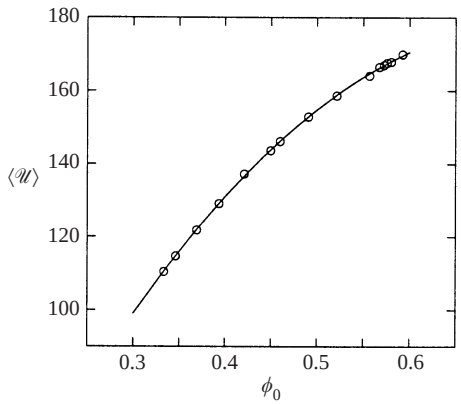

FIGURE 2. Calibration of the averaged intensity received by the camera, $\langle \mathscr{U} \rangle$, with the mean volume fraction, ϕ_0. The solid curve corresponds to the best square-law correlation.

tubes. A diffuser screen was then placed between the neon tubes and the bed in order to obtain a lighting of the bed as homogeneous as possible.

The fluidized bed was filmed at 25 frames per second. The intensity received by the camera was averaged over 400 frames, for a given square box of the camera field. We then established the calibration law giving the average intensity $\langle \mathscr{U} \rangle$ received by the camera at this given location in the bed as a function of the mean particle concentration ϕ_0. A typical result is shown in figure 2. The calibration law did not depend on the size of the box over which the averaging was performed nor on the rate of frame acquisition. The steepness of the fitting square-law depended on the aperture of the camera and on the intensity of the backlighting. For instance, if the aperture was low, the resolution in received light intensity was weak and the calibration law was flattened. In order to avoid the sparkling of the glass beads which saturated the camera, we used a sheet of tracing paper which was positioned on the bed glass wall facing the camera. The images were slightly smoothed without any sparkling.

Once the calibration law was known, we had access to the particle concentration 'map' of the flow. The camera field was divided into rectangular cells and the fitting calibration law was computed on each cell. The size of the cell, which corresponded in fact to a 'resolution', could be chosen freely. Then, each instantaneous image captured by the camera was divided into the same grid and the particle concentration for each cell was deduced from the corresponding calibration law. With this technique, it was possible to ignore any inhomogeneities in the backlighting of the bed, as they simply affect locally the calibration law. We were also able to study the particle concentration fluctuations, i.e. the standard deviation σ_ϕ of the concentration distribution at a given location in the fluidized bed, by measuring the fluctuations of the intensity received by the camera. The size of the cell did not affect the results concerning particle concentration fluctuations as long as it was smaller than 6 mm, i.e. smaller than the typical length scale of the fluctuations. The results presented in this paper were obtained by dividing the camera field into 4 mm square cells which also ensured a good resolution of processed images.

2.3. *Particle image velocimetry*

We also filmed the fluidized beads near the glass wall and particle velocities were measured using the particle image velocimetry technique (PIV). The bed was now illuminated from the front, that is from the same face as that filmed by the camera. The

camera was focused on the beads against the glass wall. For this kind of measurement, the sheet of tracing paper fixed on the glass wall was of course removed.

Series of stacks of two images were acquired. Each stack was then processed to find the velocity-vector map of the flow field by using an adapted source code and compiled application for PIV developed by Cardoso within NIH image†, see Cardoso, Marteau & Tabeling (1994). In practice, this involves discretizing each image into a map of 25×25 nodes. In a small interrogation region explored around each node, the local particle displacement between the two images was measured using direct cross-correlation techniques. This was repeated around each node to build up the complete two-dimensional velocity-vector map.

When using glass beads, the time interval between two images was 1/50 s. In fact, the two images were simply the odd and even fields of a single frame obtained with the camera. Reliable results were obtained only when the particle motion was large (typically 4–5 pixels in between two images). For smaller bead displacement, random bead sparkling between the two images generally overwhelmed the real bead displacement and thus misled the PIV application.

When using stainless steel beads, the image quality was much better than with glass beads since there was no sparkling of the metallic beads but rather a sharp reflection of the front light on each bead which acted like a tracer for the PIV application. It proved to be very reliable and efficient to measure the velocity field using the PIV technique.

3. Experimental results for moderate-density beads

3.1. *Description of the flow regimes*

As previously noted in the fluidized bed literature (see for instance Ham *et al.* 1990; Didwania & Homsy 1981), different regimes of fluidization are observed depending on the fluid superficial velocity q. Typical expansion results, obtained when plotting the superficial velocities q versus mean particle volume fractions ϕ_0, are presented in figure 3 in the case of beads of set B. This expansion curve can be well-fitted by an empirical Richardson–Zaki relation, $q = v_t(1 - \phi_0)^n$.

Below minimum fluidization, $q < q_{mf}$, the fluid crosses the packed suspension which can be considered as a porous medium. For $q > q_{mf}$, the fluidization is not homogeneous since the liquid crosses the suspension of nearly packed beads through preferential paths. This regime is called 'worming' fluidization, see Ham *et al.* (1990). The value of q_{mf} was taken to be the velocity at which the bed began to expand and was measured by identifying the break in the expansion curve, see figure 3. The exact value of q_{mf} showed a small hysteresis depending whether the transition was noticed by increasing the flow rate q progressively from zero or by decreasing q from a larger value. But the behaviour observed at a particular flow rate q did not exhibit path dependence for the regimes described below.

As the flow rate is increased, $q > q_c$, the whole suspension is fluidized and starts to exhibit a primary voidage wave instability where a concentration plane wave propagates upwards and grows along the bed. The wavefronts are horizontal and extend over the width of the cell. The particle concentration is a function of the vertical direction z. The dominant vertical wavelength λ_z is given in table 2. It does

† Both adapted source code and compiled application for PIV on MacOS are available at http://134.157.79.91/olivier/NIH/NIH.html. There is also a standard C version available at the same address for Unix or Window usage.

Set	v_t (cm s^{-1})	n	q_{mf} (cm s^{-1})	q_c (cm s^{-1})	q_{2D} (cm s^{-1})	q_t (cm s^{-1})	λ_z (cm)
A	21 ± 0.5	2.4 ± 0.03	2 ± 0.05	2.8 ± 0.1	3.6 ± 0.1	Not observed	4.0 ± 0.2
B	14 ± 0.3	2.53 ± 0.03	1 ± 0.05	1.5 ± 0.2	2.2 ± 0.1	3.8 ± 0.1	3.5 ± 0.2
D	10.3 ± 0.2	3.23 ± 0.01	0.55 ± 0.02	0.75 ± 0.02	0.88 ± 0.02	1.32 ± 0.02	2.2 ± 0.1

TABLE 2. Expansion characteristics and vertical wavelength λ_z.

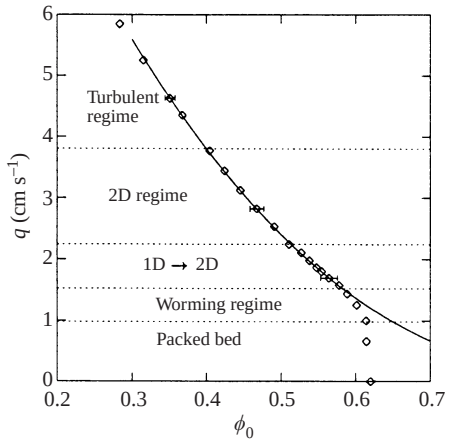

FIGURE 3. Expansion curve of the fluidized bed for beads B. The solid line corresponds to the Richardson–Zaki law.

not depend on the flow rate q. Once the wave has reached a certain amplitude, we observe the transverse destabilization of the plane wavetrain and thus the transition from a one-dimensional to a two-dimensional regime where the particle concentration is a function of both the horizontal, x, and vertical, z, directions. The aim of this paper is to study this secondary instability which will be described in more detail in the next section.

With further increase in the flow rate, the growth rate of the primary instability increases and the two-dimensional destabilization of the plane wavetrain occurs closer to the bottom of the bed. For $q > q_{2D}$, the lateral coherence of the wave is lost over all the bed height. We do not observe a stage of plane-wave growth but rather a two-dimensional structure straight away. For an even larger flow rate ($q > q_t$), the two-dimensional wavy state no longer exists and the regime is turbulent. In this regime, first described by El-Kaissy & Homsy (1976), particle concentration is homogeneous and individual particles move randomly around some mean position. Limitations of our pump did not allow us to increase the flow rate further (it was up to $q = 7\,\mathrm{cm\,s^{-1}}$) and thus we did not observe the transition to a bubbly regime, with bubbles appearing sporadically in the bed over the turbulent background, reported by Didwania & Homsy (1981).

This succession of regimes was observed for sets B and D of moderate-density beads. The turbulent regime was not found for set A, probably because of the limitation of the pump. The expansion characteristics as well as the flow rate limits between the regimes are given in table 2.

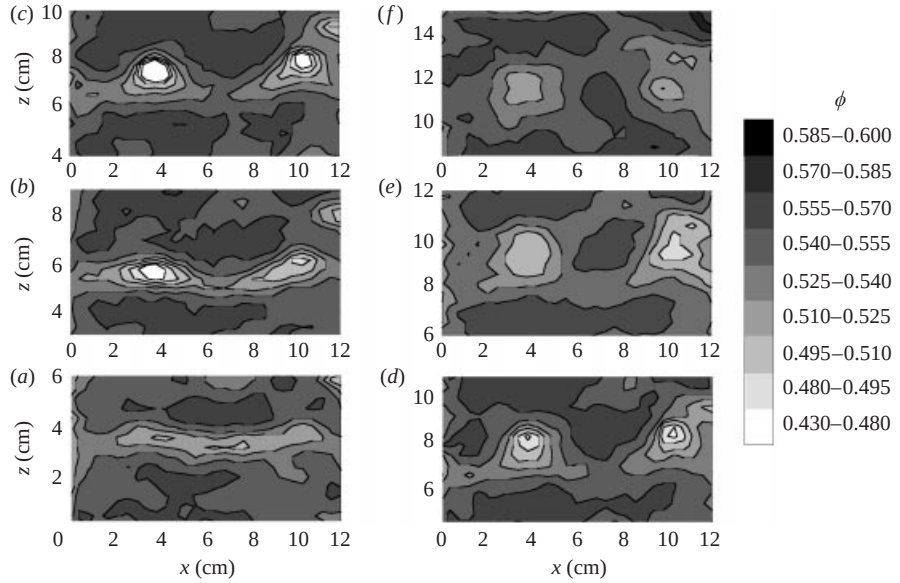

FIGURE 4. Two-dimensional destabilization of a plane wave with set A of particles, for $q = 3.1\,\mathrm{cm\,s^{-1}}$ ($\phi_0 = 0.55$). (*a*) $t = 0\,\mathrm{s}$, (*b*) $t = 0.16\,\mathrm{s}$, (*c*) $t = 0.28\,\mathrm{s}$, (*d*) $t = 0.32\,\mathrm{s}$, (*e*) $t = 0.40\,\mathrm{s}$, (*f*) $t = 0.56\,\mathrm{s}$. The 'zero' z-position is arbitrary and does not correspond to the bed bottom. The uncertainty in ϕ is ± 0.003.

3.2. *Two-dimensional destabilization*

We now describe the secondary instability of the voidage wavetrain, observed for flow rates $q_c < q < q_{2D}$. A typical transverse destabilization, obtained with beads of set A, is shown in figure 4. The same behaviour was obtained for beads of set B. These images have been processed as described in § 2.2. The two-dimensional destabilization of the plane wave can be described as a four-stage event. First, the plane wave reaches a certain amplitude which will be discussed in the following subsection, see figure 4(*a*). Secondly, the wave buckles and one or two zones of higher voidage appear. We do not observe more than one or two break-ups by plane waves in the width of our rectangular cell (two voidage pockets can be seen in figure 4*b*, *c*). This indicates that the secondary instability wavelenght λ_x is probably of the order of the width, or half the width, of the bed. A precise determination of this wavelength would necessitate a bed of wider lateral extent. Thirdly, these voidage pockets accelerate, see figure 4(*c*). The minimum particle concentration reached inside a voidage pocket during the destabilization is obtained at the very beginning of this third phase, when the voidage pocket starts to accelerate. Finally, the voidage pockets disappear, see figure 4(*d*, *e*) and no recognizable pattern was established, see figure 4(*e*, *f*) (note that the concentration variations are very weak for these last plots). It should be noticed that there is no clear distinction between the last two stages as the acceleration and the destruction of the voidage pockets happen simultaneously. We also observe that during the acceleration stage, the voidage pocket often merges with the wave just ahead, or the remnant of the wave if it has just broken up. This happens to the voidage pocket on the right in figure 4 and also results in the disappearance of the diluted blob.

The mechanism of destruction of the buoyant blob (fourth and last stage in the above discussion) can be investigated in more detail. During the last stage of

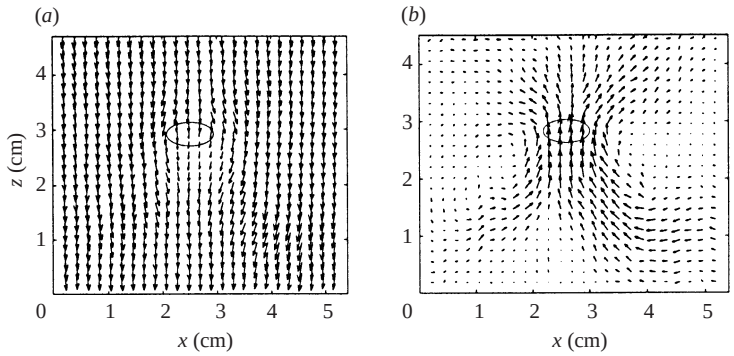

FIGURE 5. Particle flow near the wall during the last stage of a break-up event: (*a*) viewed from a reference frame moving with the buoyant blob; (*b*) viewed from the fixed laboratory frame. The position of the remaining hole of low concentration is indicated.

the typical event described above, see figure 4(*d*, *e*), we were able to perform PIV measurements despite the sparkling of the glass beads, because the motion of the beads was then significant. Unfortunately, in the earlier stages of the two-dimensional destabilization, the motion of the particles was too small and therefore no reliable PIV measurements were possible. Figure 5 shows the particle flow field near the glass wall. Figure 5(*a*) is viewed from a frame moving with the voidage pocket whereas figure 5(*b*) is viewed from the fixed laboratory frame. We located on these two graphs the low-concentration zone, similar to the one visible in figure 4(*d*). Figure 5(*b*) reveals the upward motion of the particles below the incipient bubble. However, figure 5(*a*) shows that, in the frame of the buoyant blob, particle motion remains directed downwards everywhere. This suggests that the blob is destroyed because it is filled from above: more particles fall through the upper surface of the bubble than can escape below. This causes the upward motion of the high-density region below the bubble as can be seen in figure 5(*b*).

Above this break-up zone, the bed reaches a complex two-dimensional regime shown in figure 6. The remnant of the original plane wave, out of which the voidage pockets grew, is strongly distorted by the break-up. The voidage pocket leaves behind slower arms of the initial voidage perturbations which are inclined steeply and can result in oblique travelling waves.

These oblique travelling waves are subjected to the same tranverse instability as the one-dimensional travelling waves resulting in the formation of transient voidage pockets (as can be seen in figure 6). Thus, above the one-dimensional wavetrain break-up region, a complex unsteady two-dimensional regime is observed, with oblique travelling waves interacting with each other or with transient voidage pockets. It is thus difficult to extract data for this flow regime. However, we can state that the oblique travelling waves are similar to the one-dimensional travelling waves, with comparable velocity and density profile. The typical spacing between two oblique travelling waves is comparable to the vertical wavelength λ_z of the original one-dimensional wavetrain. We observe oblique travelling waves tilted to the right or to the left. The amount of tilt is variable but never exceeds 30° (see figure 6). As the flow rate is increased, for $q_{2D} < q < q_t$, this complex two-dimensional wavy state fills all the bed height.

For the smaller beads of set D, the situation encountered for $q_c < q < q_{2D}$ is slightly different. A transverse destabilization of the voidage wavetrain is still observed but it

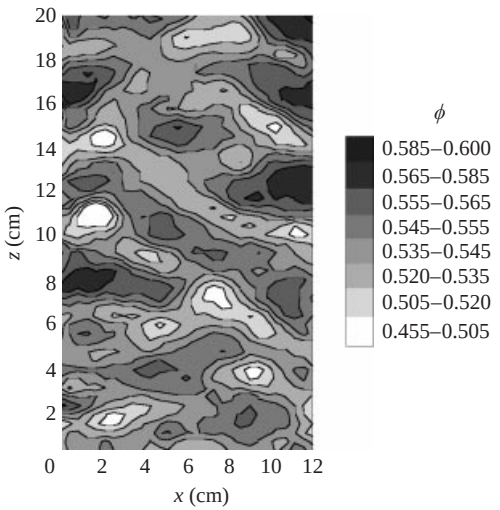

FIGURE 6. Flow regime above the break-up zone with set A of particles, for $q = 3.3\,\mathrm{cm\,s^{-1}}$ ($\phi_0 = 0.536$). The 'zero' z-position is arbitrary and does not correspond to the bed bottom. The uncertainty in ϕ is ± 0.003.

does not give birth to short-lived voidage pockets, as observed for sets A and B. It rather takes the form of a transverse modulation of the initially plane wave, which evolves smoothly. The deformed wavetrain is show in figure 7. Merging between two-dimensional waves is frequent. The same behaviour was also observed in a narrower fluidized beds with an aspect ratio $W_b/d_s \sim 90$, i.e. with same lateral confining effect as that of sets A and B in the 12 cm wide bed. This seems to show that the observed difference in two-dimensional destabilization (between beads A/B and D) is not due to different lateral confinement.

3.3. *Fluctuations of concentration*

The study of the particle-concentration fluctuations is also a way to obtain more information about the transverse destabilization. Figure 8 presents the standard deviation of the particle concentration distribution σ_ϕ for set of beads A, as a function of bed height for different flow rates q. For $q = 2.8\,\mathrm{cm\,s^{-1}}$ (circles in figure 8) the growth of the particle-concentration fluctuations is clearly exponential throughout the bed height and this is related to the slow growth of the plane wavetrain. For $q = 3\,\mathrm{cm\,s^{-1}}$ (squares in figure 8), an initial stage of exponential growth is still seen but, at 35 cm from the bed bottom, fluctuations reach a maximum and then decrease slightly. In fact, the initial increase of the fluctuations is due not only to the growth of the one-dimensional wavetrain but also to the appearance of voidage pockets, at 20–30 cm from the bottom of the bed. The small decrease happens in the bed region located just above the two-dimensional destabilization zone and is due to the 'homogenization' of particle concentration resulting from the destruction of the two-dimensional voidage pockets. For $q = 4\,\mathrm{cm\,s^{-1}}$ and $q = 6\,\mathrm{cm\,s^{-1}}$ (respectively diamonds and crosses in figure 8), the flow regime is immediately two-dimensional but we nonetheless notice a rapid increase of the particle-concentration fluctuations from the bed bottom.

First, this plot shows the existence of a saturated value σ_ϕ^{sat} for the particle-concentration fluctuations, which seems to be independent of the mean particle concentration, as already observed by El-Kaissy & Homsy (1976). It must be repeated

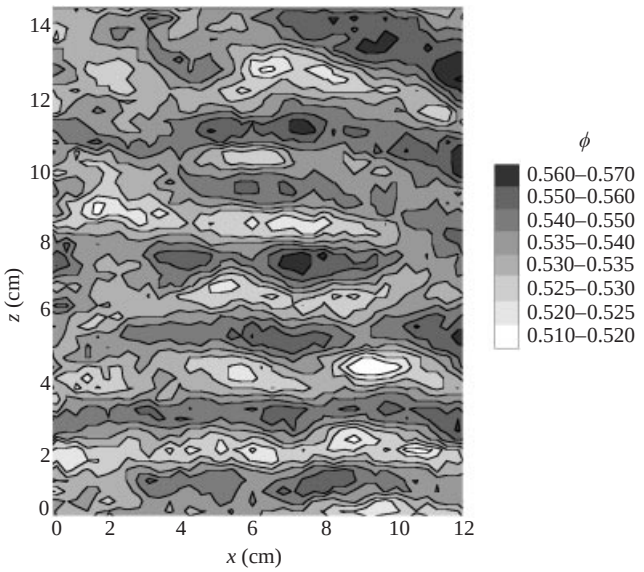

FIGURE 7. Transverse modulation of the wavetrain observed with beads D, for $q = 0.85\,\mathrm{cm\,s^{-1}}$ ($\phi_0 = 0.538$). The 'zero' z-position is arbitrary and does not correspond to the bed bottom. The uncertainty in ϕ is ± 0.003.

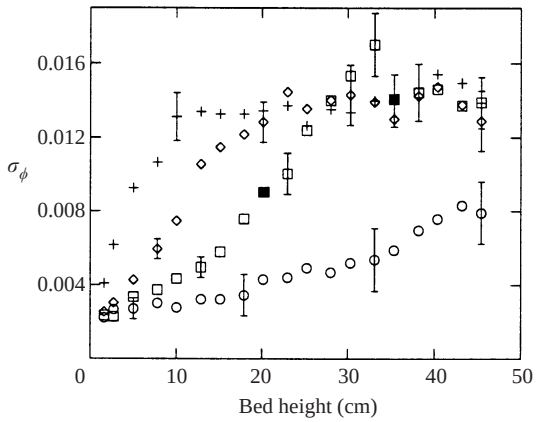

FIGURE 8. Particle concentration fluctuations, σ_ϕ, as a function of bed height, for beads A and for four different flow rates. ○, $q = 2.8\,\mathrm{cm\,s^{-1}}$ ($\phi_0 = 0.566$); □, $q = 3\,\mathrm{cm\,s^{-1}}$ ($\phi_0 = 0.558$); ■ at $z = 20\,\mathrm{cm}$ indicates the lower limit of the two-dimensional destabilization region; ■ at $z = 35\,\mathrm{cm}$ indicates the upper limit of this region, see § 3.2; ◇, $q = 4\,\mathrm{cm\,s^{-1}}$ ($\phi_0 = 0.5$); +, $q = 6\,\mathrm{cm\,s^{-1}}$ ($\phi_0 = 0.4$).

that this saturated value is obtained after the two-dimensional destabilization zone and thus corresponds to a complex two-dimensional regime. As can be seen in table 3, this value seems to depend only on the particle diameter. The value of σ_ϕ^{sat} obtained with our set A is comparable to what was measured by El-Kaissy & Homsy (1976) with a similar experimental setup and with the same beads. As the Reynolds and Froude numbers based on the fluid velocity u ($Re = ud_s\rho_f/\mu_f$, $Fr = u^2/gd_s$) were the only dimensionless groups varied independently in their experiments, El-Kaissy & Homsy argued that the statistically defined property σ_ϕ^{sat} should scale like Re^2/Fr

Set	ϕ_0-range	σ_ϕ^{sat}
A	0.40–0.57	0.014 ± 0.001
B	0.40–0.57	0.014 ± 0.001
D	0.52–0.55	0.003 ± 0.001

TABLE 3. Value of σ_ϕ^{sat} for beads A, B and D.

Set	ϕ_0	σ_ϕ^c	a_{1D}	a_{sat}
A	0.53–0.57	0.008 ± 0.001	0.023 ± 0.006	0.10–0.13
B	0.52–0.57	0.011 ± 0.001	0.032 ± 0.006	0.6–0.7
D	0.52–0.55	0.003 ± 0.001	0.009 ± 0.003	0.8

TABLE 4. Value of σ_ϕ^c for beads A, B and D. The value a_{sat} was not measured in the one-dimensional experiments for beads of set D, but the measured value of a_{sat} for beads of same the density and similar diameter (770 μm), was ~ 0.8.

to be independent of the flow rate. The present results agree approximately well with this scaling: $\sigma_\phi^{sat} \sim g d_s^3/(\rho_f/\mu_f)^2$.

Secondly, since the two-dimensional destabilization of the voidage wavetrain is the main concern of this study, we tried to estimate the value of the particle-concentration fluctuations σ_ϕ in the region of the bed where the two-dimensional destabilization occurs. For example at $q = 3\,\mathrm{cm\,s^{-1}}$, the transition from a one-dimensional regime to a two-dimensional regime occurs in a zone of 10 cm vertical extent located between $z = 20$ cm and $z = 30$ cm. Hence, fluctuations in particle concentration at $z = 20$ cm, $\sigma_\phi = 0.008 \pm 0.001$, are the expression of the presence of a purely one-dimensional wave close to destabilizing transversally. We can estimate such a *critical* value of the particle concentration fluctuations σ_ϕ^c for flow rates $q_c < q < q_{2D}$, for which a stage of one-dimensional growth is visible, see table 4. It seems not to depend on q and the corresponding limited range in ϕ_0 for which it was measured is given in table 4. From the shape of the wave deduced from the previous study of Duru *et al.* (2002), we can then relate σ_ϕ^c to the amplitude of the one-dimensional wave just before its transverse destabilization, a_{1D}, for further details see Duru (2001). This value can also be recovered from the analysis of concentration maps such as shown in figure 4. This critical one-dimensional wave amplitude is much smaller than the amplitude of a one-dimensional saturated wave, a_{sat} measured in the previous work of Duru *et al.* (2002), as can be seen in table 4. This clearly means that the destabilization of the one-dimensional wave occurs before it becomes saturated.

4. Experimental results for high-density beads

4.1. *Description of the flow regimes*

In this section, we focus on the different flow regimes observed when using set C of particles (stainless steel beads, $d_s = 1$ mm and $\rho_s = 7.8\,\mathrm{g\,cm^{-3}}$). The expansion curve for these beads is shown in figure 9. The bed of particles remains packed for $q < q_{mf}$ and a worming regime is observed for $q_{mf} < q < q_c$ (the expansion characteristics are given in table 5). As for the moderate-density beads, the primary instability observed for $q_c < q$ takes the form of a voidage wavetrain. It propagates and grows along the bed before destabilizing transversally. Figure 10 shows successive snapshots of

Set	v_t (cm s^{-1})	n	q_{mf} (cm s^{-1})	q_c (cm s^{-1})	q_b (cm s^{-1})
C	35.4 ± 0.4	2.66 ± 0.03	3.0 ± 0.05	3.7 ± 0.01	4.8 ± 0.02

TABLE 5. Expansion characteristics for beads C.

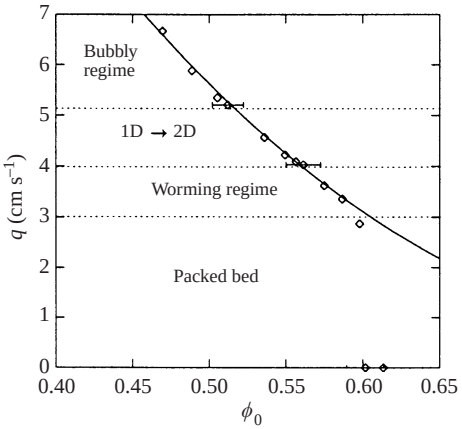

FIGURE 9. Expansion curve of the fluidized bed for beads of set C. The solid line corresponds to the Richardson–Zaki law.

the fluidized beads visible at the wall during a typical destabilization event. The fluidized bed is not only lit from behind but also from the front: each white spot is the reflection of the front light on a single bead. As the motion of the beads due to the voidage wave is very small and so there are no blurred parts on the pictures (the shutter time is 1/50 s), we present next to each snapshot a sketch in order to outline the position of the voidage perturbation.

The destabilization of the plane perturbation seen in figure 10(*a*) results in the buckling of the plane wave, see figure 10(*b*), and gives birth to a voidage pocket (see figure 10*b*, *c*). We have no way, with our set-up, to measure the particle concentration in the dilute region. However, the backlight is visible through the voidage hole so that it must be extremely dilute. The void accelerates and its size increases as it starts to propagate up the bed, see figure 10(*d*, *e*). The similarity between this succession of events and what was obtained for moderate-density beads A and B, see § 3.2, is striking. The first stages of the two-dimensional destabilization, namely the buckling of the voidage wave, the appearance of a dilute zone and its acceleration, are similar. The major difference lies in the evolution of the dilute structure created by the secondary instability. For glass beads, we can hardly use the term 'bubble', in the usual fluidized bed terminology, to describe the buoyant blob obtained as it is far from being totally empty of particles and disappears very quickly. But with beads of set C, we obtain a propagating structure empty of particles, as can be seen in figure 10(*e*), that is a real bubble. To our knowledge, our experiments are the first to report bubble formation resulting clearly from the destabilization of a one-dimensional voidage perturbation.

For $q_c < q < q_b$, the life-time of such a bubble is very short as it is rapidly destroyed when colliding with remnants of plane waves or other bubbles. But as the flow rate is increased, for $q_b < q$, the bed behaviour becomes clearly dominated by the bubble

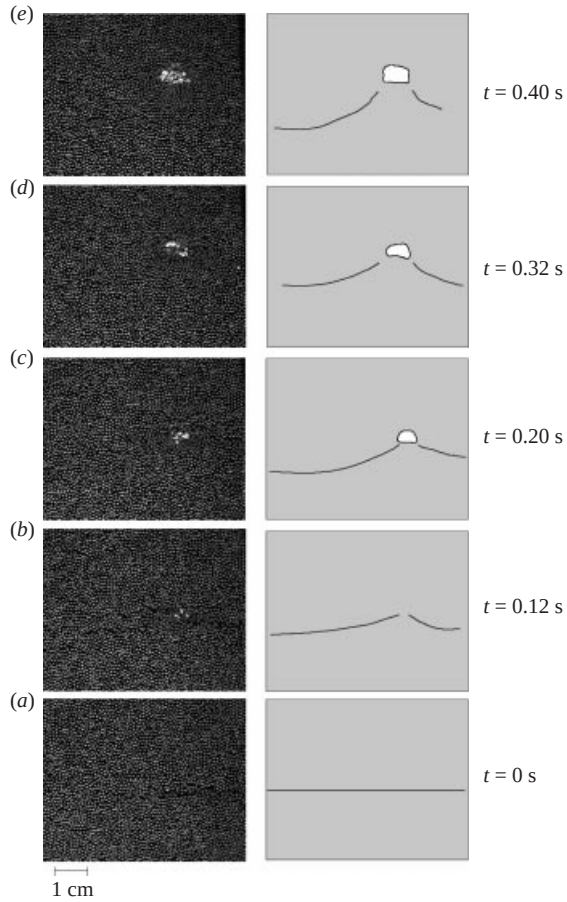

FIGURE 10. Transverse destabilization of a plane voidage wave with beads C. The sketches on the right show the position of the voidage perturbation.

dynamics. In this bubbly regime, bubbles appear continually within the bed. They result from the destabilization of plane waves near the bottom of the bed. For such flow rates, the lateral extent of these plane waves is a few centimetres and they do not extend over the bed width. Higher in the bed, the strong agitation caused by the bubble motion also creates density fluctuations susceptible to evolving into bubbles. A new-born bubble has a continuously increasing size. Bubbles are not stationary two-dimensional structures. A typical bubble picture is shown in figure 11(*a*). The shutter time is 1/50 s and the blurred parts of the picture make apparent the particle motion around the bubble. In figure 11(*b*), we show the particle flow field around a bubble obtained by PIV (in the fixed laboratory frame) to emphasize the particle motion seen in figure 11(*a*). The bubble has an almost circular shape with a rounded top and a flat bottom, like a bubble in a gas-fluidized bed.

4.2. *Bubbly regime*

There is an extensive amount of literature on the bubbling regime observed in gas-fluidization, in two-dimensional and three-dimensional geometry (for a review, see Davidson 1995). It is thus interesting to compare the characteristics of the bubbly regime we observe in our liquid-fluidized bed to those obtained in gas fluidization.

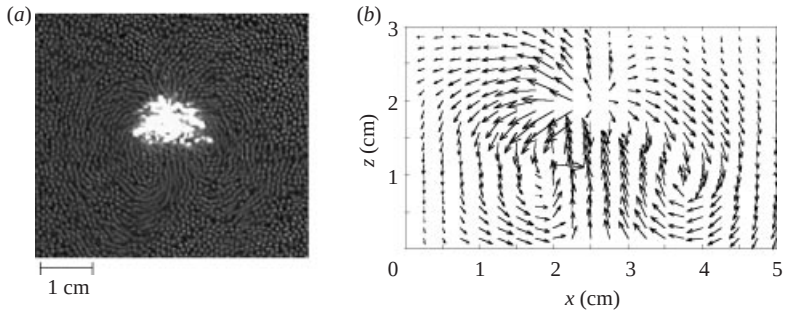

FIGURE 11. (*a*) Bubble picture; (*b*) particle flow around a bubble, obtained by PIV.

4.2.1. *Bubble behaviour*

As already mentioned, newly formed bubbles have a rapidly increasing size. This individual bubble growth is also encountered in gas fluidization. A bubble breaks up into two parts once it has reached a critical size. Such a bubble break-up event is shown in figure 12. As the bubble propagates (see figure 12*a*, *b*), its size increases and its shape tends to widen, see figure 12(*c*). Then falling particles make an indentation at the top of the bubble and this causes the elongated bubble to separate into two smaller bubbles (figure 12*d*). This happens only once the bubble reaches some critical lateral extent. Depending on the relative size of each fragment, both bubbles may continue to propagate or the smaller may disappear as it cannot grow if it is hindered by the larger. This latter situation occurs in figure 12(*e*, *f*). The remaining bubble continues to propagate and starts growing again: it will soon break up into two parts. As a consequence of this break-up mechanism, we do not observe the progressive formation of bubbles of larger and larger size. It must be mentioned that the same kind of bubble splitting mechanism is observed in gas fluidization (in two-dimensional and three-dimensional beds), see Rowe (1971). To our knowledge, the only theoretical approach to the bubble splitting problem is due to Clift, Grace & Weber (1974), who treated the upper interface bubble-dense phase as an interface undergoing a Rayleigh–Taylor instability. However, their results do not predict a maximum stable size for a bubble that could be compared to experimental results.

In the bubbly regime observed in our liquid-fluidized bed, when two bubbles come closer, they start following one each other, forming 'trains' of bubbles. Within these 'trains', the distance between two adjacent bubbles remains more or less constant. The bubbles are strongly distorted and their rise speed is larger than that of an isolated bubble. Figure 13 shows such a 'train' of bubbles. Three bubbles are visible within the camera field. The number of bubbles involved in a train (and so its vertical extent) is variable but can be large. The typical spacing between two successive bubbles is 4–7 cm. 'Trains' of bubbles propagate until they reach the surface of the bed. The particles between two bubbles of the same train experience a large upward motion, as shown by the blurred zone in figure 13. Therefore, the 'trains' induce strong recirculation motions of the particles within the bed. Such bubble flow patterns are also encountered in gas-fluidized beds, see Clift & Grace (1985).

4.2.2. *Statistics of the bubbles size*

We have studied the bubble-size distribution and its evolution along the vertical direction z. For a given value of z, 500 images of the bed are captured. The capture window, of dimensions 3×12 cm, is centred on the given z-value. The total number

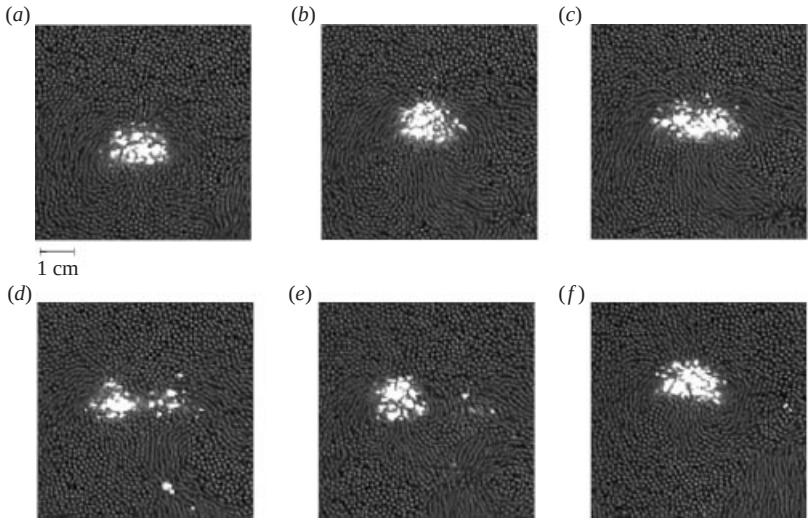

FIGURE 12. Bubble splitting. (*a*) $t = 0$ s, (*b*) $t = 0.12$ s, (*c*) $t = 0.16$ s, (*d*) $t = 0.28$ s, (*e*) $t = 0.36$ s, (*f*) $t = 0.52$ s.

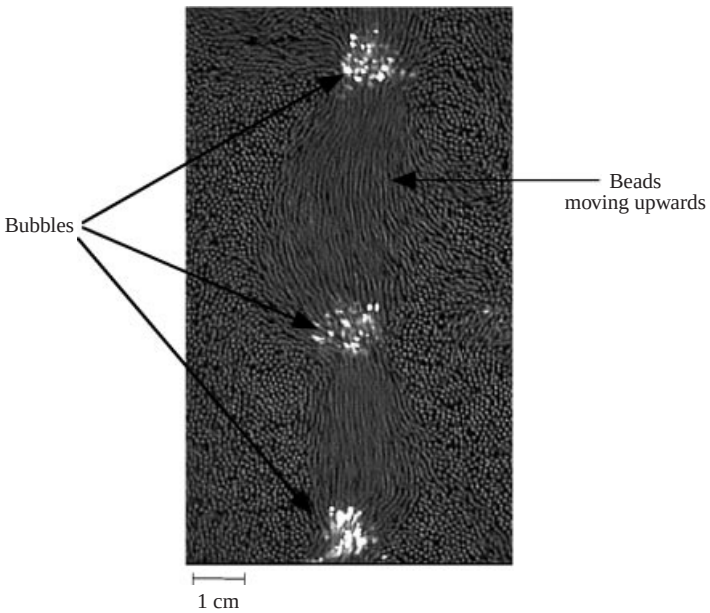

FIGURE 13. A 'train' of bubbles.

of bubbles and the bubble-area distribution are then measured using the software NIH Image, see Duru (2001) for further details. Figure 14 shows the evolution with z of the distribution of bubble area A, expressed in cm^2. For a given z, we have plotted the percentage of the total number of bubbles in each of four area categories. The inset shows the total number of bubbles as a function of z. These measurements were made in the bubbly regime, for $q = 5.2\,\mathrm{cm\,s^{-1}}$ (figure 14*a*) and $q = 4.4\,\mathrm{cm\,s^{-1}}$ (figure 14*b*). The statistical distribution of bubble area remains unchanged as long as $z > 25\,\mathrm{cm}$ for $q = 5.2\,\mathrm{cm\,s^{-1}}$ and $z > 35\,\mathrm{cm}$ for $q = 4.4\,\mathrm{cm\,s^{-1}}$, which confirms the visual observation that there is no global growth of bubble size along the bed. Also,

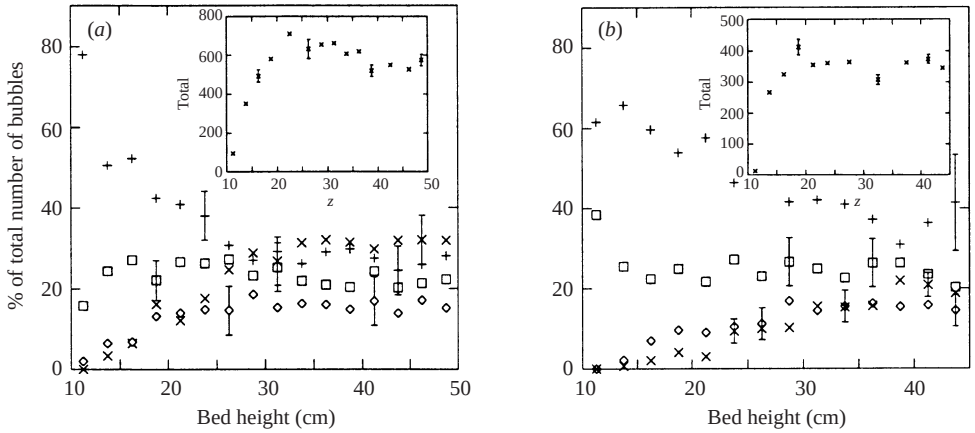

FIGURE 14. Bubble area A distribution as a function of z. (*a*) $q = 5.2\,\mathrm{cm\,s^{-1}}$; (*b*) $q = 4.4\,\mathrm{cm\,s^{-1}}$. $0.3200 < A < 0.6300$ (+); $0.6300 < A < 0.9500$ (□); $0.9500 < A < 1.2600$ (◇); $1.2600 < A$ (×). A is expressed in $\mathrm{cm^2}$. The inset gives the evolution of the total number of bubbles as a function of z.

the total number of bubbles remains constant. At a flow rate $q = 5.2\,\mathrm{cm\,s^{-1}}$ and for $z > 25\,\mathrm{cm}$, the mean bubble radius, defined by half the maximal lateral extent of the bubble and measured on video images, is $0.7 \pm 0.1\,\mathrm{cm}$. The observed bubbles do not have exactly a circular shape (see for instance figure 11). Bubble aspect ratio, defined by $2r_b/h_b$ (where h_b is the maximal vertical extent of the bubble and is measured on video images) ranges between 1.3 and 1.5.

These data suggest that in our fluidized bed of limited height, one can nonetheless talk about a fully developed state of bubbling where the number of bubbles and bubble size distribution depends only on q. It results from a dynamic equilibrium between bubble growth and formation on one hand and bubble splitting on the other hand.

4.2.3. *Rise velocity of the bubbles*

The rise velocity of bubbles has been widely studied in gas-fluidized beds. It has been shown experimentally that for an isolated bubble in a three-dimensional bed:

$$u_b = K(gr_b)^{1/2}, \tag{4.1}$$

where the constant K depends on the fluidized material (typically K ranges between 0.8 and 1, see Rowe 1971). Some theoretical analyses of single bubble motion in a gas-fluidized bed (for a review, see Jackson 2001), taking advantage of the fact that $\rho_f \ll \rho_s$ in this case, and based on two-phase equations, have shown that $u_b = 2/3(gr_b)^{1/2}$ (the prefactor 2/3 is replaced by 1/2 in a two-dimensional case).

The velocity of an isolated bubble in a gas-fluidized bed thus compares well to the velocity of the Davies–Taylor (see Davies & Taylor 1950) spherical-cap bubble of the same radius r_b:

$$u_b = \tfrac{2}{3}[gr_b(1 - \rho_i/\rho_o)]^{1/2}, \tag{4.2}$$

where ρ_i denotes the density of the material within the bubble and ρ_o the density of the material outside (the prefactor 2/3 is again replaced by 1/2 in a two-dimensional case). In the gas-fluidized bed case, $\rho_i = \rho_f \ll \rho_o \sim \rho_s$.

In order to measure the rise velocity of a bubble in our liquid-fluidized bed, we evaluate the bubble displacement between two video pictures of the bed, separated

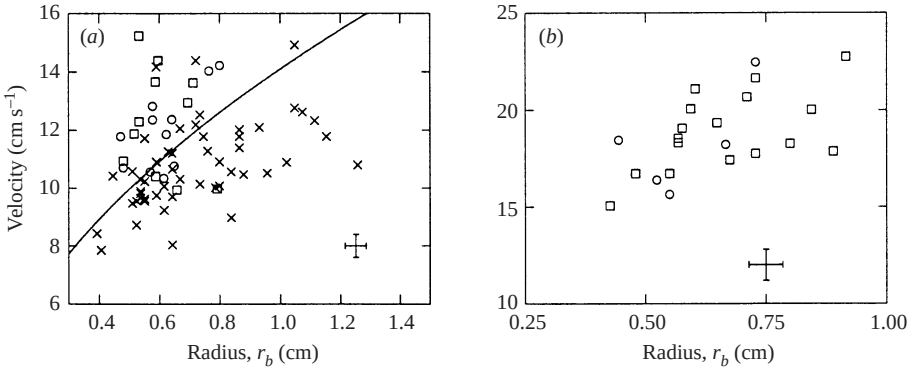

FIGURE 15. Rise velocity of bubbles as a function of the bubble radius r_b: (*a*) results for isolated bubbles: $q = 4.0\,\mathrm{cm\,s^{-1}}$ (×), $q = 4.8\,\mathrm{cm\,s^{-1}}$ (○), $q = 5.7\,\mathrm{cm\,s^{-1}}$ (□), the curve corresponds to equation (4.3); (*b*) results for bubbles in 'trains': $q = 4.8\,\mathrm{cm\,s^{-1}}$ (○), $q = 5.7\,\mathrm{cm\,s^{-1}}$ (□).

by a known time interval. This time interval is short (typically 0.5 s) so that the size of the bubble, characterized by its radius r_b, can be considered as constant. We make a distinction between isolated bubbles and bubbles in a 'train'. These measurements were made for $q = 4.8\,\mathrm{cm\,s^{-1}}$ and $q = 5.7\,\mathrm{cm\,s^{-1}}$, in the bubbly regime, and at $q = 4\,\mathrm{cm\,s^{-1}}$. In this last case, bubbles were 'injected' in the bed with the forcing device described in § 2.1, by imposing a strong voidage perturbation at the bottom of the bed. The large-amplitude perturbation rapidly breaks up which results in a pair of bubbles. The advantage of this technique is that it simplifies greatly the observation of *isolated* bubbles. Indeed, for a flow rate q slightly larger than the critical flow rate q_c, the fluidized suspension displays a slow growth of one-dimensional voidage waves. The bubbles injected at the bottom of the bed are therefore more likely to cover long distances without interacting with pronounced voidage perturbations or other bubbles, resulting from one-dimensional wave destabilization. This type of technique is similar to that used in gas-fluidized beds, when some gas is injected through the bed support to give birth to isolated bubbles.

Figure 15(*a*) presents the experimental results on the velocity of isolated bubbles. The solid curve corresponds to the following equation:

$$u_b = 0.5[g r_b(1 - \rho_i/\rho_o)]^{1/2}, \tag{4.3}$$

where $\rho_i = \rho_f$ and $\rho_o = (1 - \phi_0)\rho_f + \phi_0\rho_s$ with $\phi_0 = 0.55$. It shows that a straightforward use of a 'Davies–Taylor like' formula provides a good estimate for the rising velocity of an isolated bubble in the liquid fluidized bed case also. For a given bubble radius, the velocity increases noticeably with the flow rate q. It has been argued by Davidson (see for instance Davidson 1995) that the actual bubble rise velocity U_b is equal to $q - q_{mf} + u_b$, where u_b is the velocity of an isolated bubble. In the present paper, u_b is much larger than $q - q_{mf}$. However, the difference seen in the rise velocities at different q seems comparable to $q - q_{mf}$.

Figure 15(*b*) shows experimental results concerning the rising velocity of bubbles within a 'train'. This velocity is approximately 1.3–1.5 times the velocity of an isolated bubble of the same size.

5. Destabilization of a high-amplitude one-dimensional perturbation

As already mentioned in § 2.1 the support of the fluidized suspension can be moved. A rapid up-and-down motion of this piston creates a local deficit of particles at the

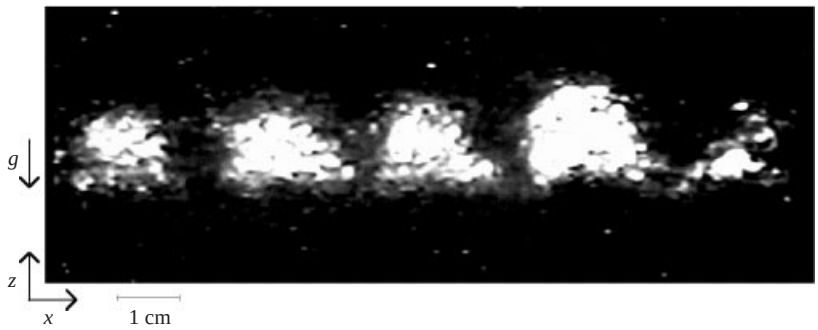

FIGURE 16. Injected bubbles with beads A, resulting from the destabilization of a high-amplitude perturbation, imposed at the bottom of the bed.

bottom of the bed, which is then convected by the flow. The displacement of the support (of typical amplitude $5d_s$) thus results in an imposed high-amplitude voidage perturbation, much larger than the critical one-dimensional wave amplitude a_{1D}. We studied the response of the bed to this single forced perturbation. The main results are summarized in this short section.

For high-density beads, at $q > q_c$, the break-up of this perturbation produces bubbles which behave like those growing from natural voidage disturbances (as mentioned in § 4.2.3). We note here that for $q < q_c$, the voidage perturbation break-up still gives birth to bubbles but these bubbles are dampened: the bubble size slowly decreases and finally the bubble disappears.

For moderate-density beads of set A, the break-up of the voidage perturbation produces the bubble-like structures seen in figure 16. Such structures are similar to the bubbles observed with high-density beads. We emphasize that such structures are never observed naturally: they are much more dilute than the buoyant blobs observed after the transverse destabilization of the one-dimensional voidage wave. For $q < q_c$, these two-dimensional structures are dampened but the poor quality of the bed pictures and interactions between these injected bubbles do not allow us to detect a specific mechanism leading to their disappearance. For $q > q_c$, contrary to what happens with high-density beads, such injected bubbles never propagate along the bed and are again dampened until their amplitude reaches the typical voidage wave amplitude. The resulting voidage perturbation then continues to propagate as a usual voidage wave. Again, the damping mechanism of these bubbles is not clear from our experiments.

Nonetheless, our experiments show that for beads A, injected bubbles do not propagate indefinitely in a bed where they do not grow 'naturally' from voidage perturbations. They also show the existence of a mechanism of destruction of the bubbles, the understanding of which could help clarify the physical mechanisms at work during the first stages of the 'natural' two-dimensional destabilization and responsible for the disappearance or the growth of the buoyant blob (depending on the bead density).

6. Comparison with previous numerical and theoretical predictions

First, we can try to compare the results concerning the destabilization of the one-dimensional wave with the prediction of the linear theory of Batchelor & Nitsche. Batchelor & Nitsche studied the stability of a fluid with density modulated sinusoidally

Beads	a_{1D}	ρ_s (g cm^{-3})	$\Delta\rho_{eq}$ (g cm^{-3})
A	0.023 ± 0.006	4.08	0.071 ± 0.016
B	0.032 ± 0.006	2.48	0.047 ± 0.010
D	0.009 ± 0.003	2.55	0.014 ± 0.004

TABLE 6. Critical wave amplitude and equivalent density stratification.

in the vertical direction: $\rho = \rho_0 + \Delta\rho \sin(\kappa z)$. For a two-dimensional unbounded stratified fluid, the stratification is always unstable (Batchelor & Nitsche 1991) but in the presence of lateral walls, there is a critical stratification (Batchelor & Nitsche 1993). The analogy with a fluidized bed is that the fluid equivalent to the fluidized suspension presents a vertical density variation resulting from the variations in particle concentration due to the one-dimensional voidage wave instability. This analogy would be applicable a liquid-fluidized bed with solid particles of density comparable with that of the liquid and/or of small size, i.e. with a small particle Reynolds number based on the relative velocity of the two phases, so that the relative dynamics of the solid dispersed phase and of the fluid phase may be neglected. This is the case neither in our experiments nor in Anderson *et al.*'s (1995) simulations; moreover such fluidized beds may proved to be stable (see Ham *et al.* 1990 and Duru *et al.* 2002). However, Anderson *et al.* (1995) found that the Batchelor–Nitsche stability analysis provides an easy way to estimate the time scale of the secondary instability of a fluidized bed, when a fully developed one-dimensional wave is destabilized laterally. Following the same idea, one can examine whether the Batchelor–Nitsche mechanism could provide a way to estimate the critical amplitude of the one-dimensional wave when the two-dimensional destabilization occurs. If this is the case, a first consequence would be that the critical stratification $\Delta\rho_{eq} = a_{1D}(\rho_s - \rho_f)$ should be independent of the sets of beads. We see in table 6 that this is not the case so that further calculations are useless.

Göz & Sundaresan (1998) studied the stability of one-dimensional waves to small, transverse two-dimensional disturbances. They calculated the critical amplitude ϵ_c, when the one-dimensional wave becomes unstable to transverse perturbations. Their results suggest that ϵ_c is very small, $\sim O(10^{-3}$–$10^{-6})$, which is much smaller than the measured a_{1D}. Such a discrepancy could be explained by the fact that their weakly nonlinear calculations depend on the assumption that the one-dimensional wave is of small amplitude. In the experiment, the critical wave amplitude a_{1D} is large (although smaller than the one-dimensional saturated value), which could mean that nonlinear effects are important when the two-dimensional destabilization occurs, which is beyond the scope of Göz & Sundaresan's paper.

We now compare our experimental results concerning the two-dimensional instability of the one-dimensional voidage wavetrain to numerical results obtained by Anderson *et al.* (1995) and Glasser *et al.* (1997). These authors performed fully nonlinear numerical simulations of the two-phase model which should be able to reproduce the experimental observations. As already mentioned, they investigated two different cases. On one hand, they have simulated the growth of a two-dimensional perturbation from the uniform unstable bed. On another hand, they studied the transverse destabilization of a large-amplitude, saturated one-dimensional wave. In § 3.2, we have seen that the experimental situation is somewhere in between the two cases studied in these numerical simulations. A purely one-dimensional growth is

	Set A	Set B	ASJ (1995)	GSK (1997)
d_s (mm)	1.2	1.2	1	1
ρ_s (g cm^{-3})	4.08	2.48	2.2	2.2
c_{1D} (cm s^{-1})	5.5 ± 0.3	4 ± 0.2	3.1	2.86
c_{2D} (cm s^{-1})	9–12	6–9	8.5	3.75
ΔT (s)	0.8–1.2	1–1.4	2.5	2
a_{1D}	0.023 ± 0.006	0.032 ± 0.006	0.3	0.22
ϕ_{min}	0.4 ± 0.05	0.4 ± 0.05	0.15	0.2
ϕ_0	0.53–0.57	0.52–0.555	0.57	0.57
Size (cm × cm)	1.5 × 1.5	1.5 × 1.5	3 × 2	1.2 × 1.2

TABLE 7. Comparison between experiments and numerical simulations. Data on the simulations were extracted from the work of Anderson *et al.* (1995) (figure 17 in their paper) and Glasser *et al.* (1997) (figure 19 in their paper).

visible in the experiments but the two-dimensional destabilization occurs 'early' in the one-dimensional wave development, before it has reached its saturated amplitude. The existence of this stage of purely one-dimensional growth preceding the two-dimensional destabilization is also backed up by previous experiments (El-Kaissy & Homsy 1976) and by the theoretical work of Göz & Sundaresan (1998). In the following therefore, we have decided to limit to the comparison to the numerical results obtained when a one-dimensional saturated wave is destabilized transversally, keeping in mind that the wave amplitude in the simulations is then much larger than in the experiment.

We first focus on the case of non-bubbly beds, namely results obtained with beads of sets A and B, and compare them to what is found in numerical simulations when a one-dimensional saturated voidage wave is allowed to destabilize transversally. The typical destabilization event depicted in figure 4 is very similar to what is found in the numerical simulations. The most satisfying point of comparison concerns the general succession of the destabilization event. The two-dimensional destabilization of the one-dimensional plane wave computed by Anderson *et al.* (1995) or Glasser *et al.* (1997) follows the same stages as those observed in the experiment: buckling, acceleration and finally homogenization of the particle concentration, see figure 17 of Anderson *et al.* (1995) and figure 19 of Glasser *et al.* (1997). Moreover, in a frame moving with the buoyant blob, Anderson *et al.* (1995) found no upward motion of solid particles at any moment during the course of the event, which seems to be confirmed by our results, compare figure 5(*a*) and figure 19 of Anderson *et al.* (1995). They concluded that the blob was filling up from above, as observed in the present experiment.

In table 7, we give the values of some experimental quantities measured in the experiment and compare them to the corresponding quantities found in the simulations of Anderson *et al.* (1995) and Glasser *et al.* (1997). The aim of this table is to go further than the qualitative similarities stressed above. The velocities c_{1D} and c_{2D} are respectively the one-dimensional voidage wave speed and the rise velocity of the two-dimensional buoyant blob. Both were measured by constructing spatio-temporal diagrams with images of the fluidized bed. The one-dimensional voidage wave is not saturated in amplitude but it has been shown (Duru *et al.* 2002) that its velocity does not change much while growing and so we believe that it is relevant to compare it to the saturated wave speed obtained in the simulations. As the lifetime of the buoyant

blob was very short, its speed is difficult to evaluate with accuracy on a spatio-temporal diagram. Thus, we only give a rough estimate for c_{2D}. The time ΔT gives an estimate of the duration of the whole destabilization event, from the initial buckling of the wave to the final homogenization. Corresponding values from simulations are taken from captions of figure 17 of Anderson *et al.* (1995) and 19 of Glasser *et al.* (1997). The amplitude a_{1D} is the already mentioned estimate of the critical value of the one-dimensional wave amplitude just before the two-dimensional destabilization and is compared to the saturated value of the one-dimensional wave amplitude used in the numerical simulations. The concentration ϕ_{min} is the minimum particle concentration reached during the break-up. It is obtained when the voidage pocket starts to accelerate and it was evaluated using our particle concentration 'maps'. The experimental figures do not depend on the mean particle concentration ϕ_0. The range in ϕ_0 for which these quantities were measured is also given in the table. The numerical results were obtained at a given value of ϕ_0, shown in the table. Finally, we compare the size of the two-dimensional structures obtained in the experiments to those obtained in the simulations.

The time scale ΔT and the velocities c_{1D} and c_{2D} are in good agreement, although the values for c_{2D} are much smaller in the simulations of Glasser *et al.* (1997). Of course, a noteworthy difference between experiments and simulations is the value of a_{1D}, as already explained. This may explain why the minimum particle concentration obtained during the simulated destabilization event is much smaller than the experimental value, since, when the simulated destabilization occurs, the difference in particle concentration between dense and dilute regions is already very large. It also could explain why the whole event, from buckling to homogenization, lasts a little longer in the numerical simulations, as it takes more time to fill the deeper concentration hole. The sizes of the transient dilute structures found in the simulations depend on the numerical scheme but give in both cases a good estimate of the real experimental size.

We now focus on the case of bubbling liquid-fluidized beds. The experimental results obtained with stainless steel beads of set C can be compared to what is obtained in the case of lead shot beads fluidized by water, studied by Glasser *et al.* (1997) ($d_s = 1\,\mathrm{mm}$, $\rho_s = 11.8\,\mathrm{g\,cm^{-3}}$). The main point is that the two-dimensional destabilization of the plane wave now results into the formation of real bubbles. We again note the similarity between the general succession of events leading to the bubble formation in the simulation (see figure 17 of the paper by Glasser *et al.* 1997) and in the experiment (see figure 10). The whole destabilization event, from the initial buckling of the plane wave to the formation of the bubble is very short in the experiment: it lasts less than one second. This contrasts with the simulation where the bubble is obtained in 9 s. However, this comparison of the time scale has to be made with care. In the simulation, the system reaches a two-dimensional stationary state (the bubble) whereas in the experiments, the bubbles are not stationary structures. Their size grows more rapidly when the flow rate q is large, as mentioned in § 4.2, until they split into two parts.

7. Conclusion

In this paper, we have presented experimental results concerning the secondary instability of the voidage wavetrain resulting from the primary instability of a uniform liquid-fluidized bed. In all cases studied, the voidage wavetrain is unstable. The most revealing results are obtained with bead sets A, B and C which have approximately

the same diameters but different densities. Whereas the two-dimensional destabilization of the voidage wave results into the formation of short-lived buoyant blob for the moderate-density beads of sets A and B, it leads to real bubble formation for high-density beads of set C, see §§ 3 and 4. In this last case, it is, as far as we know, the first time that the complete succession of instabilities leading to bubble formation has been observed experimentally. The difference between moderate- and high-density beads arises during the evolution of the dilute blob that appeared as a result of the two-dimensional destabilization. Whereas it rapidly fills in from above with moderate-density beads, its size rapidly increases with high-density beads, which leads to the obtaining of a real bubble. This nonlinear stage of the secondary instability seems to be well-captured by nonlinear simulations of the two-phase model, especially for moderate-density beads. However, a clear physical understanding of this difference is still lacking. Our experiments reveal that the difference between bubbling and non-bubbling systems is not absolute as previously indicated by Anderson *et al.* (1995). But numerical simulations with intermediate ratio ρ_s/ρ_f, for instance ranging from 4 to 10, could clarify this point by focusing on the relative motion of particles and fluid at the very beginning of the dilute blob formation.

We should mention that in the present experiment, the destabilization of the one-dimensional wave is permitted only in the wider transverse x-direction because of the small depth of the bed. In a fully three-dimensional bed, we may anticipate that the destabilization will happen in both horizontal directions.

The estimate of the one-dimensional wave critical amplitude is also an important result, see § 3.3. The prediction of this secondary instability threshold is a challenging problem for theory. A 'simple' argument, involving a critical density stratification of the fluid equivalent to the suspension, inspired by the work of Batchelor and Nitsche, fails. It also seems unlikely that a weakly nonlinear theory may be used. Indeed, in our relatively narrow bed, the estimated critical wave amplitude is large. In a wider bed, transverse destabilization may occur earlier in the one-dimensional wave development, as the apparatus can then contain longer transverse unstable modes (see Göz & Sundaresan 1998). It then may be possible to compare the critical wave amplitude to theory. This could also be studied in two-dimensional simulations where the limited lateral extent of the system is taken into account. More generally, future numerical simulations should study the influence of the one-dimensional wave amplitude on the two-dimensional destabilization process. For instance, the study of the destabilization of high-amplitude voidage perturbation could make clear the physical mechanisms at work, as suggested by the results obtained when a large perturbation is applied, see § 5.

Finally, the observation of a bubbly regime in the case of high-density beads, for $\rho_s/\rho_f \approx 8$, is a new feature of liquid–solid fluidization, see § 4.2. It should motivate new theoretical and numerical studies based on the two-phase equation of motion in which terms involving ρ_f are no longer neglected, which could help the understanding of some striking features of bubbles such as the particle flow pattern, 'trains' of bubbles, and bubble splitting.

We would like to thank E. J. Hinch and M. Nicolas for discussions, O. Cardoso for the use of his PIV application and F. Ratouchniak, J.-C. Morellini and P. Cervetti for technical assistance. This work is part of the thesis of P. Duru sponsored by the French Ministère de l'Éducation Nationale, de la Recherche et de la Technologie.

REFERENCES

Anderson, T. B. & Jackson, R. 1968 Fluid mechanical description of fluidized beds. Stability of the state of uniform fluidization. *Ind. Engng Chem. Fundam.* **7**, 12–21.

Anderson, T. B. & Jackson, R. 1969 Fluid mechanical description of fluidized beds. Comparison of theory and experiments. *Ind. Engng Chem. Fundam.* **8**, 137–144.

Anderson, K., Sundaresan, S. & Jackson, R. 1995 Instabilities and the formation of bubbles in fluidized beds. *J. Fluid Mech.* **303**, 327–366.

Batchelor, G. K. 1988 A new theory of the instability of a uniform fluidized bed. *J. Fluid Mech.* **193**, 75–110.

Batchelor, G. K. 1993 Secondary instability of a gas-fluidized bed. *J. Fluid Mech.* **257**, 359–371.

Batchelor, G. K. & Nitsche, J. M. 1991 Instability of stationary unbounded stratified fluid. *J. Fluid Mech.* **227**, 357–391.

Batchelor, G. K. & Nitsche, J. M. 1993 Instability of stratified fluid in a vertical cylinder. *J. Fluid Mech.* **252**, 419–448.

Batchelor, G. K. & Nitsche, J. M. 1994 Expulsion of particles from a buoyant blob in a fluidized bed. *J. Fluid Mech.* **278**, 63–81.

Cardoso, O., Marteau, D. & Tabeling, P. 1994 Quantitative experimental study of the free decay of quasi two dimensional turbulence. *Phys. Rev.* E **49**, 454–461.

Clift, R. & Grace, J. R. 1985 Experimental properties of bubbles. In *Fluidization* (ed. J. F. Davidson, R. Clift & D. Harrison), 2nd edn, chap. 3. Academic.

Clift, R. Grace, J. R. & Weber, M. E. 1974 Stability of bubbles in fluidized beds. *Ind. Engng Chem. Fundam.* **13**, 45–51.

Davidson, J. F. 1995 Fluidized particles and bubbles in fluidized beds. In *Mobile Particulate Systems* (ed. É. Guazzelli & L. Oger). NATO ASI Series E, vol. 287, pp. 173–220. Kluwer.

Davidson, J. F. & Harrison, D. 1963 *Fluidized Particles.* Cambridge University Press.

Davies, R. M. & Taylor, G. I. 1950 The mechanics of large bubbles rising through extended liquids and through liquids in tubes. *Proc. Ry. Soc. Lond.* A **200**, 375.

Didwania, A. K. & Homsy, G. M. 1981 Flow regime and flow transitions in liquid-fluidized beds. *Intl J. Multiphase Flow* **7**, 563–580.

Duru, P. 2001 Lois constitutives et instabilités en fluidisation liquide-solide. Thèse de Doctorat de l'Université de Provence.

Duru, P., Nicolas, M., Hinch, E. J. & Guazzelli, É. 2002 Constitutive laws in liquid-fluidized beds. *J. Fluid Mech.* **452**, 371–404.

El-Kaissy, M. M. & Homsy, G. M. 1976 Instability waves and the origin of bubbles in fluidized beds. Part 1: experiments. *Intl J. Multiphase Flow* **2**, 379–395.

Glasser, B. J., Kevredikis, I. G. & Sundaresan, S. 1996 One- and two-dimensional travelling wave solutions in gas-fluidized beds. *J. Fluid Mech.* **306**, 183–221.

Glasser, B. J., Kevredikis, I. G. & Sundaresan, S. 1997 Fully developed travelling wave solutions and bubble formation in fluidized beds. *J. Fluid Mech.* **334**, 157–188.

Göz, M. F. 1995 Transverse instability of plane voidage wavetrains in gas-fluidized beds. *J. Fluid Mech.* **303**, 55–81.

Göz, M. F. & Sundaresan, S. 1998 The growth, saturation, and scaling behaviour of one- and two-dimensional disturbances in fluidized beds. *J. Fluid Mech.* **362**, 83–119.

Ham, J. M., Thomas, S., Guazzelli, É., Homsy, G. M. & Anselmet M.-C. 1990 An experimental study of the stability of liquid-fluidized beds. *Intl J. Multiphase Flow* **16**, 171–185.

Homsy, G. M., El-Kaissy, M. M. & Didwania, A. 1980 Instability waves and the origin of bubbles in fluidized beds. Part 2: comparison with theory. *Intl J. Multiphase Flow* **6**, 305–318.

Jackson, R. 2001 *Dynamics of Fluidized Particles.* Cambridge University Press.

Nicolas, M., Chomaz, J.-M., Vallet, D. & Guazzelli, É. 1996 Experimental investigations on the nature of the first wavy instability in liquid-fluidized beds. *Phys. Fluids* **8**, 1987–1989.

Rowe, P. N. 1971 Experimental properties of bubbles. In *Fluidization* (ed. J. F. Davidson & D. Harrison), chap. 4. Academic.